Supporting Information

The DNA cleavage and opening reactions of human topoisomerase IIα are regulated *via* Mg^{2+}-mediated dynamic bending of gate-DNA

Sanghwa Lee, Seung-Ryoung Jung, Kang Heo, Jo Ann W. Byl, Joseph E. Deweese, Neil Osheroff, & Sungchul Hohng

Content:

SI Materials and Methods

Single-molecule measurements. To prevent nonspecific adsorption of enzyme, quartz microscope slides and coverslips were cleaned, coated with polyethylene glycol (m-PEG-5000; Laysan Bio Inc.), and biotinylated PEG (biotin-PEG-5000; Laysan Bio, Inc.) with 40:1 ratio. DNA duplexes were immobilized on the PEG-coated surface via a streptavidin-biotin interaction (1). Single-molecule fluorescence images were taken in a home-built prism-type total-internal-reflection fluorescence microscope with 50-ms or 1-s time resolution. All measurements were performed at 22 ^{o}C with the following buffer composition unless mentioned otherwise: 10mM Tris-HCl (pH 8.0), 135 mM KCl, 5 mM $MgCl_2$, 5 nM enzyme and an oxygen scavenger system (0.4 % (w/v) glucose (Sigma), 1 mM Trolox (Sigma), 1 mg/ml glucose oxidase (Sigma), 0.04 mg/ml catalase (Roche)) to slow photobleaching (2). Enzyme was diluted 100–fold for the 5 nM experiments, or 50–fold for the 10 nM experiments. Therefore, the imaging buffer also contains as much diluted components of the enzyme storage buffer (50 mM Tris (pH 7.7), 5 mM DTT, 1 mM NaEDTA, 750 mM KCl, 40 % (v/v) glycerol). As an excitation source, a green laser (532-nm, Compass215M, Coherent) was used. Fluorescence signals from Cy3 and Cy5 were collected by a water immersion objective (UPlanSApo 60x; Olympus), filtered through 532-nm long-pass filter (LP03-532RU-25; Semrock), separated with a dichroic mirror (635dcxr; Chroma Technology), and imaged on an EM-CCD camera (Ixon DV897, Andor). In buffer exchange experiments, a new buffer was infused in real time into the detection chamber by using a syringe pump (PHD 22/2000; Harvard Apparatus) while single-molecule images were being taken. For calculation of FRET efficiency, which was defined as the ratio of acceptor intensity to the sum of donor and acceptor intensities, background subtraction, and bleed-through correction of the donor signal to the acceptor channel were done, but gamma correction was not performed.

Determination of kinetic rates. Association/dissociation and bending/straightening rates were determined by the combination of threshold method and eye inspection of fluorescence intensity and FRET time traces, respectively. Dwell time histograms of each state thus obtained were fit by an exponential decay function to obtain corresponding kinetic rates. Since DNA duplexes have two competing reaction pathways of bending and dissociation in the presence of Mg^{2+} ions, the duration time histograms of enzyme-bound state without bending give the sum of bending and dissociation rates, which is multiplied by the relative frequency of each event to obtain individual rates of bending and dissociation rates (3)

References

1. Roy R, Hohng S, & Ha T (2008) A practical guide to single-molecule FRET. *Nat Methods* 5(6):507-516.
2. Rasnik I, McKinney SA, & Ha T (2006) Nonblinking and long-lasting single-molecule fluorescence imaging. *Nat Methods* 3(11):891-893.
3. Nahas MK, *et al.* (2004) Observation of internal cleavage and ligation reactions of a ribozyme. *Nat Struct Mol Biol* 11(11):1107-1113.

Fig. S1. DNA duplexes used in this work

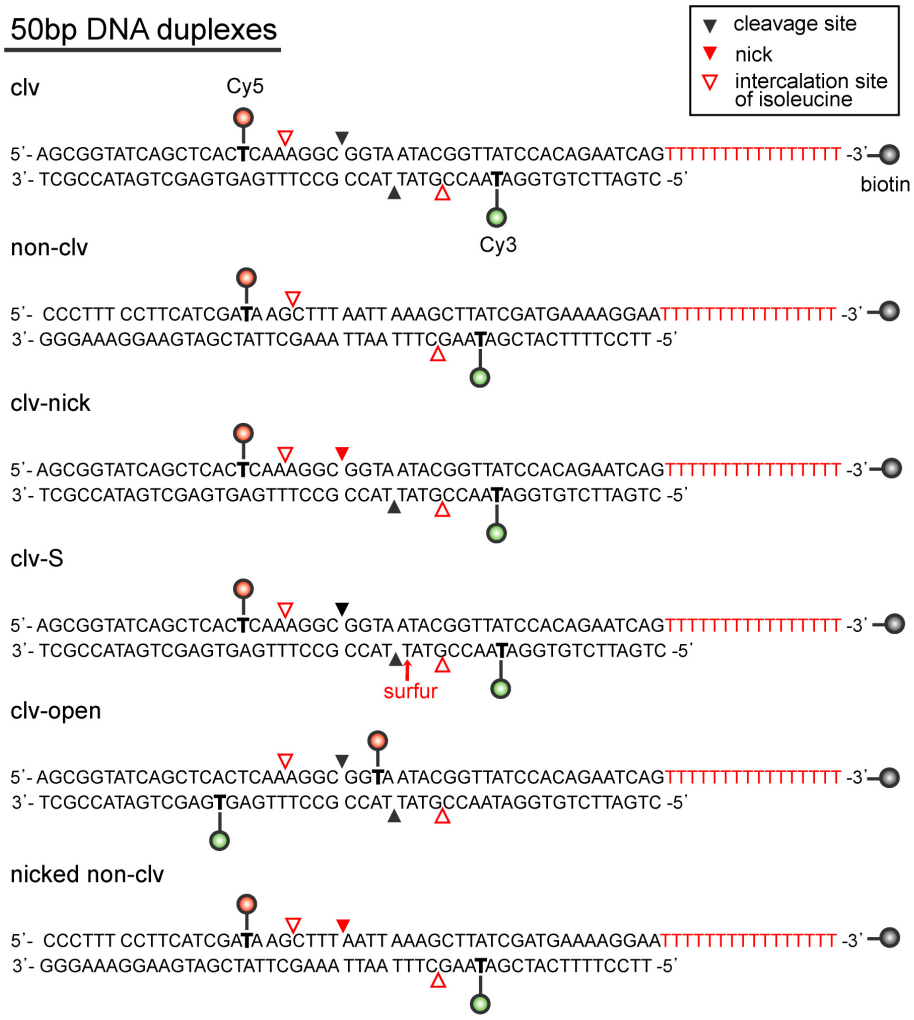

Fig. S2. Fluorescence intensity and FRET time traces in the absence of enzyme

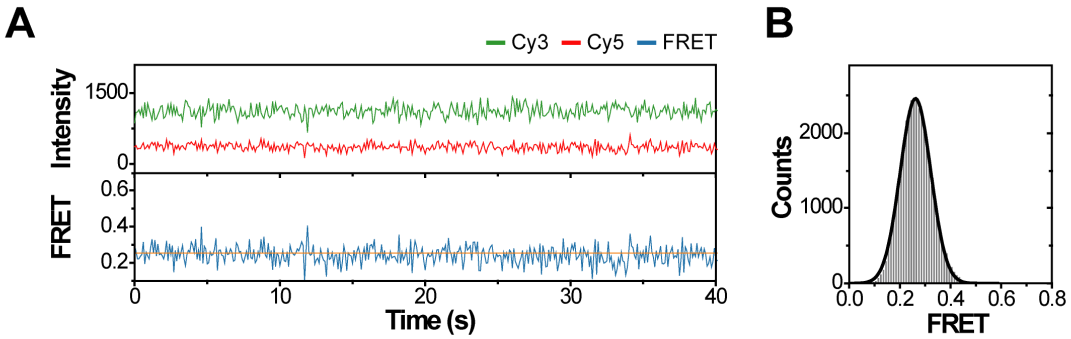

(A) Representative fluorescence intensity (top) and FRET (bottom) time traces of clv in the absence of enzyme. (B) FRET histogram of clv in the absence of enzyme.

Fig. S3. Association and dissociation times of clv in the absence of Mg^{2+}

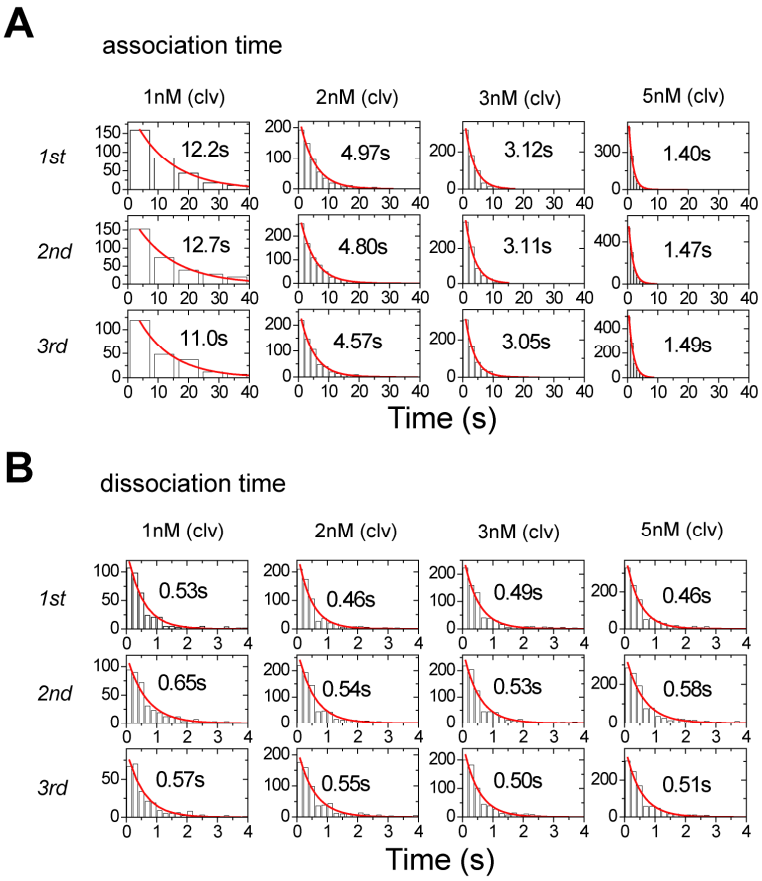

(A) Association time histograms of clv at varying enzyme concentrations. To obtain error bars in Fig. 1D, each experiment was repeated three times. (B) Dissociation time histograms of clv at varying enzyme concentrations. To obtain error bars in Fig. 1E, each experiment was repeated three times. Each histogram was fit by single-exponential function to obtain the corresponding kinetic rate. Experiments were performed without divalent ions.

Fig. S4. Bulk measurement of the DNA equilibrium binding curve

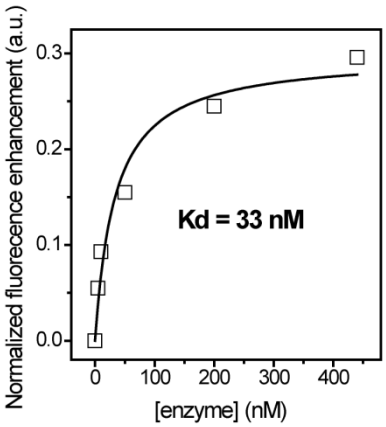

Measurements were generated using a Varian Cary Eclipse fluorescence spectrophotometer. The sample was excited at 530-nm to obtain fluorescence emission spectra. The reaction buffer contained 9.5 mM Tris-HCl (pH 8.0), 0.5 mM DTT, 1 mM NaEDTA, 142.5 mM KCl, 4 % glycerol. DNA substrate (clv, 1 nM) was mixed with varying enzyme concentrations and incubated for 5 min before measurements. Fluorescence enhancements due to PIFE (protein-induced fluorescence enhancement) were determined by the normalized difference between Cy3 emission peaks before and after the injection of designated concentrations of enzyme. To obtain dissociation constant, the data were fit to the following quadratic equation (Mueller-Planitz, F. & Herschlag, D. *J Biol Chem* **281**, 23395-23404 (2006)).

$$I_{obs} = I_{bound} \cdot \left(\frac{[D] + [E] + \mathrm{K}_d - \sqrt{([D] + [E] + \mathrm{K}_d)^2 - 4 \cdot [D] \cdot [E]}}{2 \cdot [D]} \right)$$

, where I_{obs}, I_{bound}, K_d, $[D]$, and $[E]$ are the observed fluorescence enhancement, the fluorescence enhancement of DNA bound to enzyme, dissociation constant, DNA concentration, and enzyme concentration, respectively. We obtained 33 nM as the dissociation constant, which is close to that determined in single-molecule measurements under similar but not identical experimental conditions (15 nM).

Fig. S5. Association and dissociation times at varying K^+ concentration

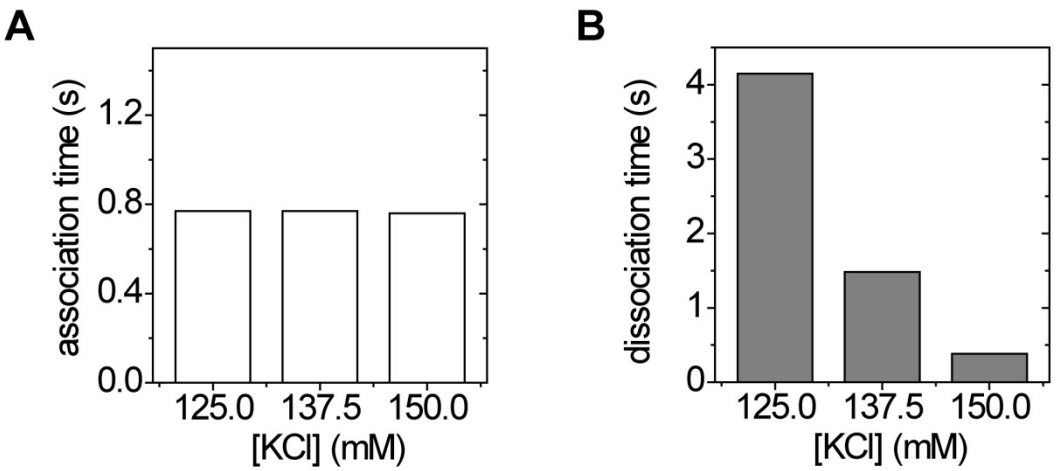

(A) Association times at varying K^+ concentration. (B) Dissociation times at varying K^+ concentration. Experiments were performed using 5 nM hTopoIIα in the absence of divalent ion.

Fig. S6. Ca^{2+}-induced DNA bending

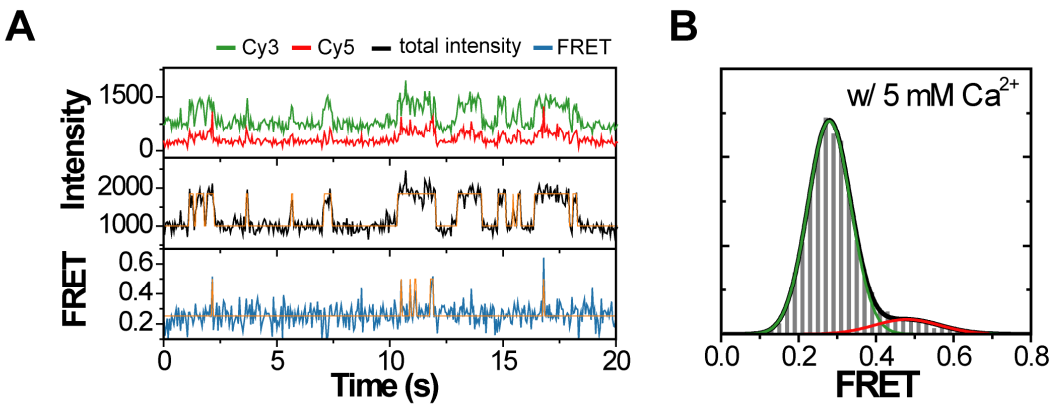

(A) Representative fluorescence intensity (top and middle) and FRET (bottom) time traces of clv in the presence of 5 nM hTopoIIα and 5 mM Ca^{2+}. (B) Corresponding FRET histogram of DNA duplex with bound enzyme in the presence of 5 mM Ca^{2+}. Histograms were fit to two Gaussian functions.

Fig. S7. Association/dissociation and bending/straightening rates in the presence of 5 mM Mg^{2+}

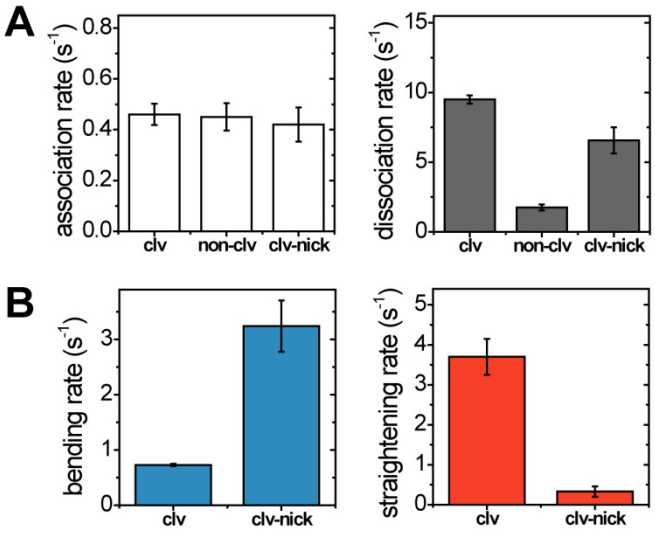

(A) Comparison of association and dissociation rates of the three DNA duplexes in the presence of 5 mM Mg^{2+} and 5 nM hTopoIIα. (B) Comparison of bending and straightening rates of the two DNA duplexes in the presence of 5 mM Mg^{2+} and hTopoIIα (5 nM).

Fig. S8. The effect of a nick in a non-cleavable sequence

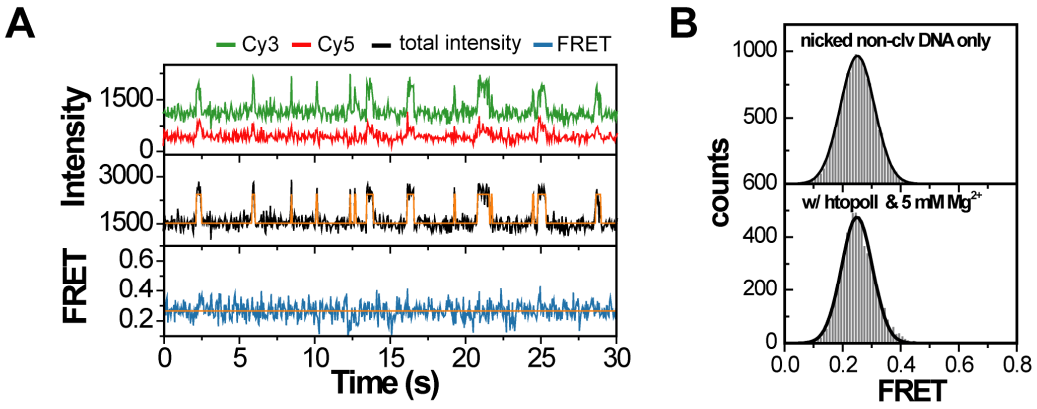

(A) Representative fluorescence intensity (top and middle) and FRET (bottom) time traces of nicked non-clv (Fig. S1) in the presence of 5 nM hTopoIIα and 5 mM Mg^{2+}. (B) Comparison of FRET histograms (top: DNA only without the enzyme, bottom: with the enzyme and 5 mM Mg^{2+}) of nicked non-clv. Histograms were fit to Gaussian functions.

Fig. S9. Association and dissociation times of non-clv and clv-nick in the absence of Mg^{2+}

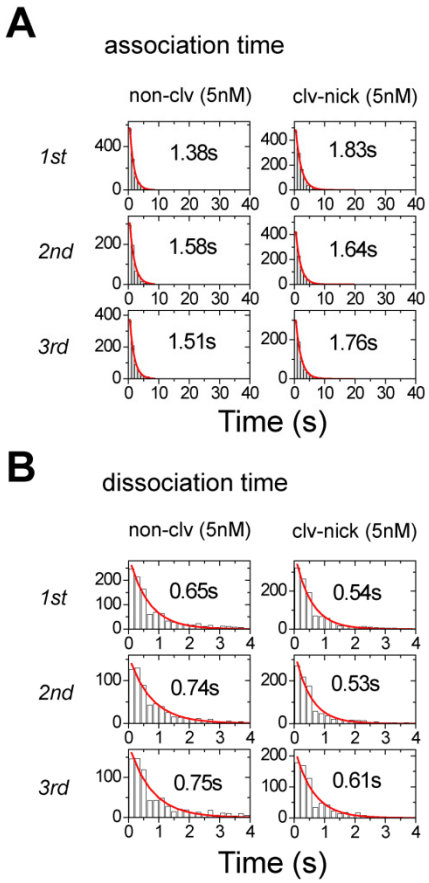

(A) Association time histograms of non-clv and clv-nick at 5 nM enzyme concentration. To obtain error bars in Fig. 2B, each experiment was repeated three times. (B) Dissociation time histograms of non-clv and clv-nick at 5 nM enzyme. Experiments were performed without divalent ions. To obtain error bars in Fig. 2C, each experiment was repeated three times.

Fig. S10. Trapping of cleavage complex at varying etoposide concentrations

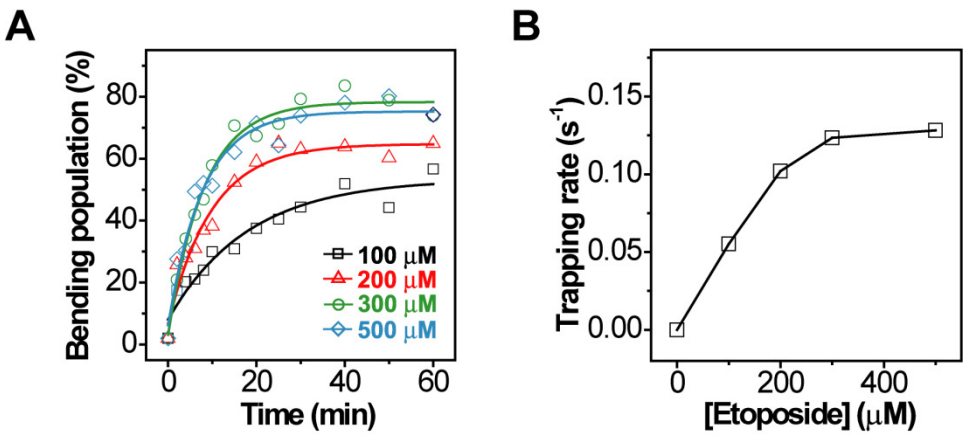

(A) Relative populations of cleavage complex as a function of incubation time at varying etoposide concentrations. (B) Trapping rates of cleavage complex as a function of etoposide concentration. Experiments were performed with 10 nM hTopoIIα, 5 mM Mg^{2+}, and designated etoposide concentration.

Fig. S11. Time-lapse FRET histograms of clv after the injection of etoposide

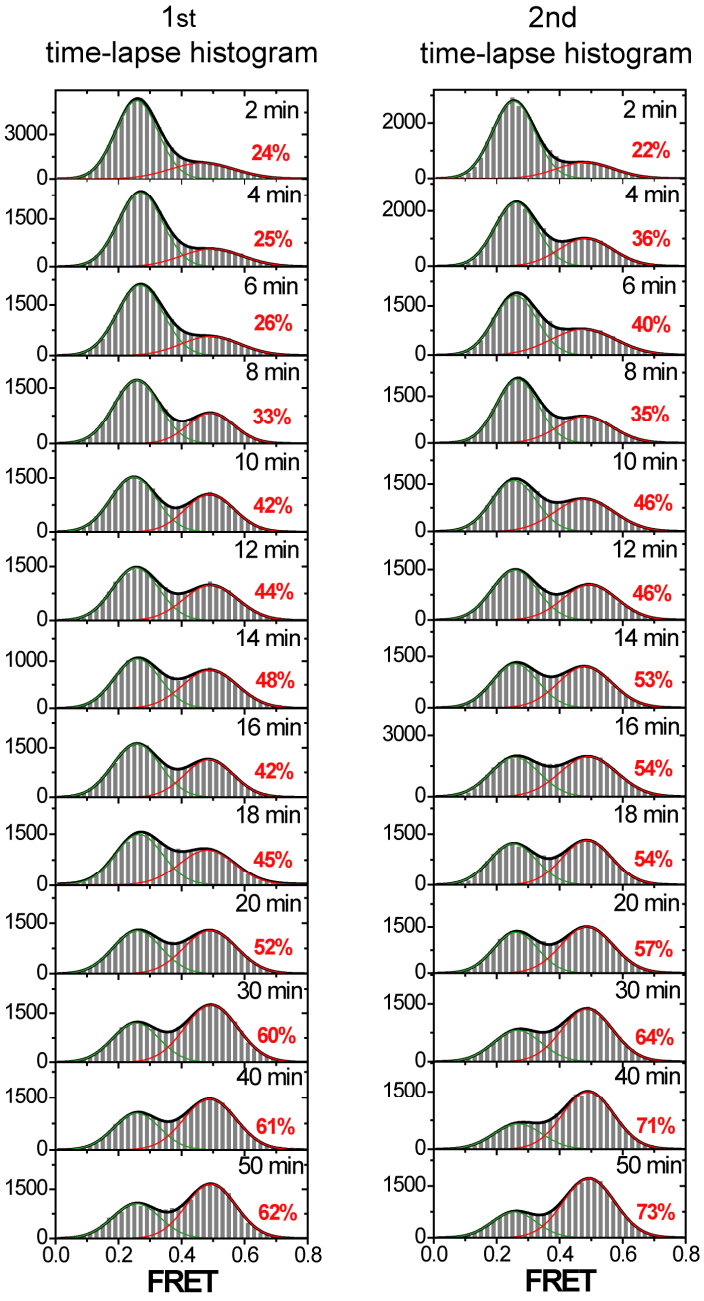

FRET histograms were made from more than 200 molecules by collecting FRET values of the first 100 frames of each molecule. All histograms were fit to the sum of two Gaussian functions to obtain relative populations of the cleavage state. Experiments were performed with 5 nM hTopoIIα, 5 mM Mg^{2+}, and 500 μM etoposide. Each experiment was repeated twice to make error bars in Fig. 2E.

Fig. S12. DNA bending by Y805F

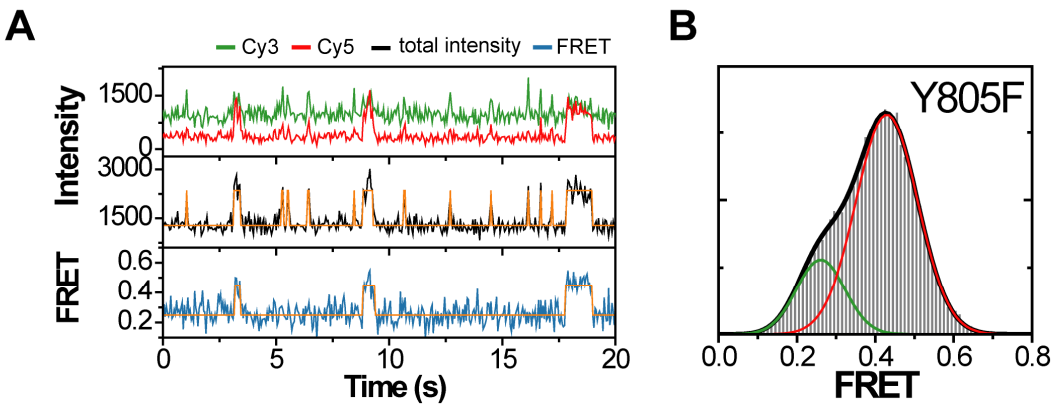

(A) Representative fluorescence intensity (top and middle) and FRET (bottom) time traces of clv in the presence of 5 nM Y805F. (B) FRET histogram of clv in the presence of 5 nM Y805F. Experiments were performed with 5 nM Y805F and 5 mM Mg^{2+}.

Fig. S13. Bending of G-segment DNA by cysteine mutants of human topoisomerase IIα

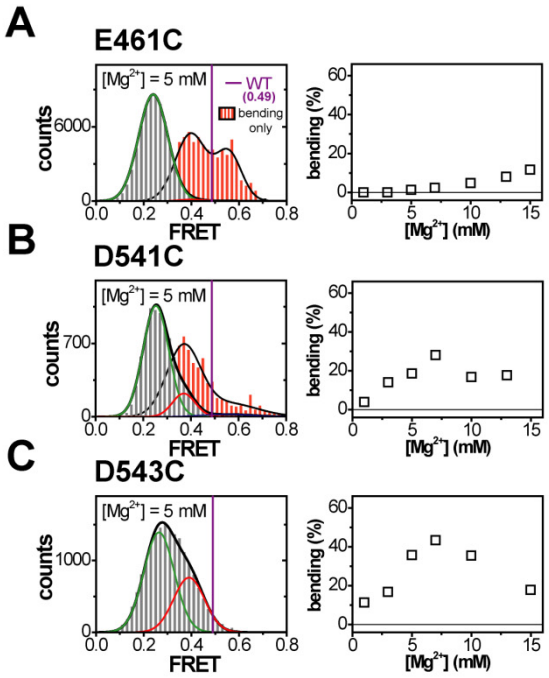

(A-C) (left) FRET histograms in the presence of 5 mM Mg^{2+} and (right) bending populations at varying Mg^{2+} concentrations of E461C (A), D541C (B), and D543C (C). In the histograms, bending only populations (red) are overlaid for clear visualization of FRET values in bent states.

Fig. S14. Time-lapse FRET histograms of clv-S after the addition of enzyme

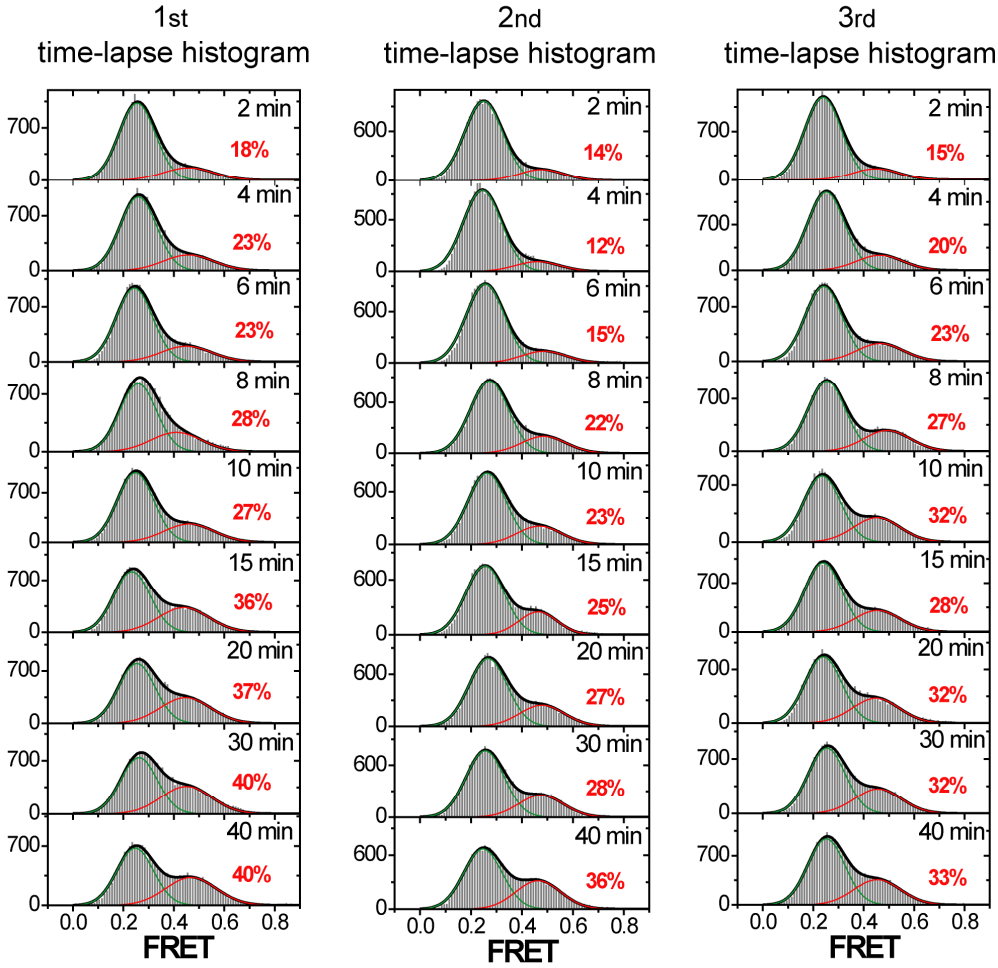

FRET histograms were made from more than 200 molecules by collecting FRET values of the first 100 frames of each molecule. All histograms were fit to the sum of two Gaussian functions to obtain relative populations of the cleavage state. Experiments were performed with 10 nM hTopoIIα and 5 mM Mg^{2+}. Experiments were repeated three times to make error bars in Fig. 4C.

Fig. S15. Direct observation of long-lived bent states

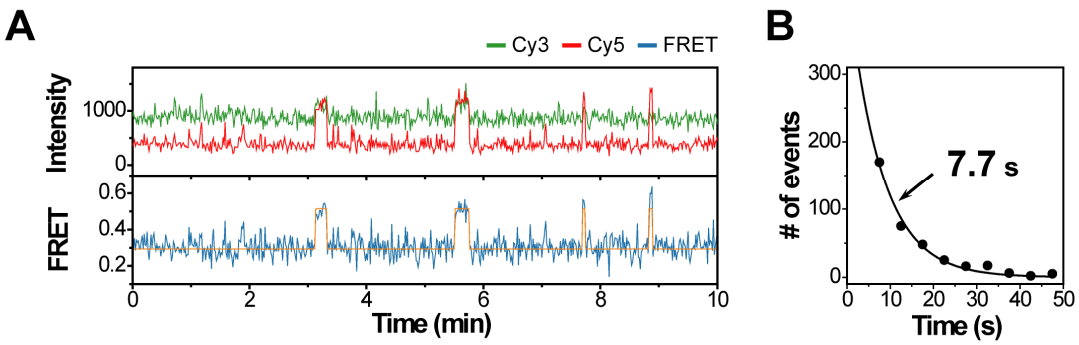

(A) Representative fluorescence intensity (Top) and FRET (Bottom) time traces of clv in the presence 5 mM Mg^{2+}. Experiment was performed with 1-s time resolution. (B) Corresponding bending lifetime histogram of clv. The data were fit to single exponential decay function (solid line) to obtain average bending lifetime.

Fig. S16. A nick at the scissile bond of one DNA strand greatly increases the bending life-time

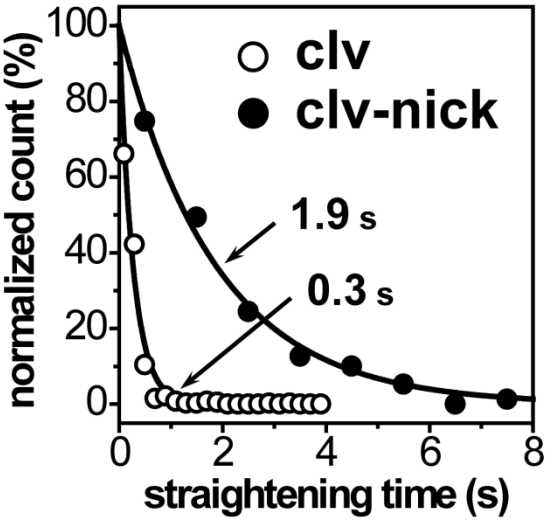

Bending lifetime histograms of clv (open circles) and clv-nick (solid circles). The data were fit to single-exponential functions (solid lines) to obtain bending life-times.

Fig. S17. Association/dissociation and bending/straightening rates of clv with or without AMPPNP

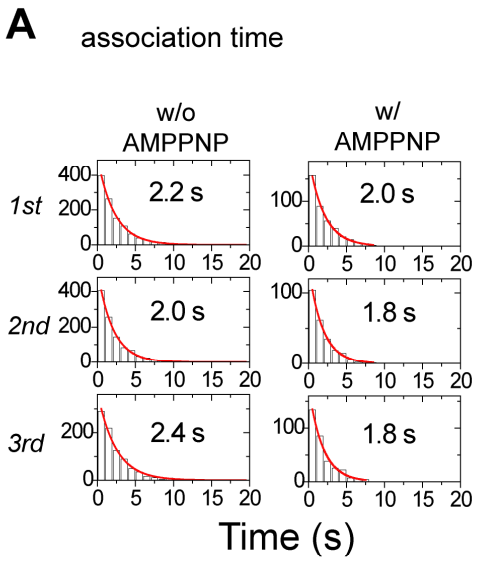

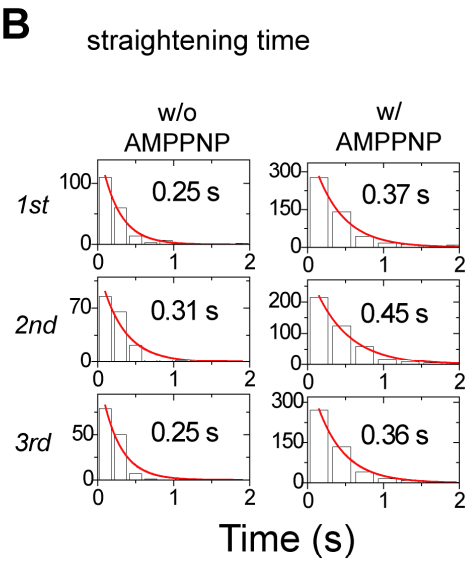

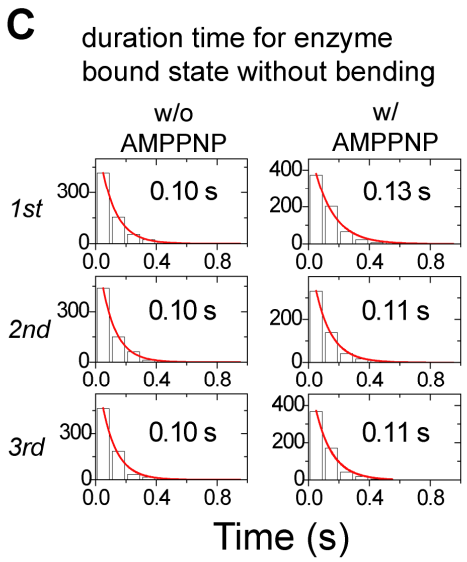

D

ratio between populations of molecules which follows bending and dissociation

condition	bending freq. / dissociation freq.
w/o AMPPNP	0.077
w AMPPNP	2.017

Histograms of association time (A), straightening time (B), and duration time of enzyme-bound state without bending (C) of clv with and without AMPPNP (1 mM). Each histogram was fit to single-exponential function to obtain kinetic rates. Experiments were performed with 5 nM hTopoIIα and 5 mM Mg^{2+}. Each experiment was repeated three times to obtain error bars in Fig. 5C. (D) Relative frequency of bending and dissociation events with and without AMPPNP.

Fig. S18. Ensemble cleavage assay

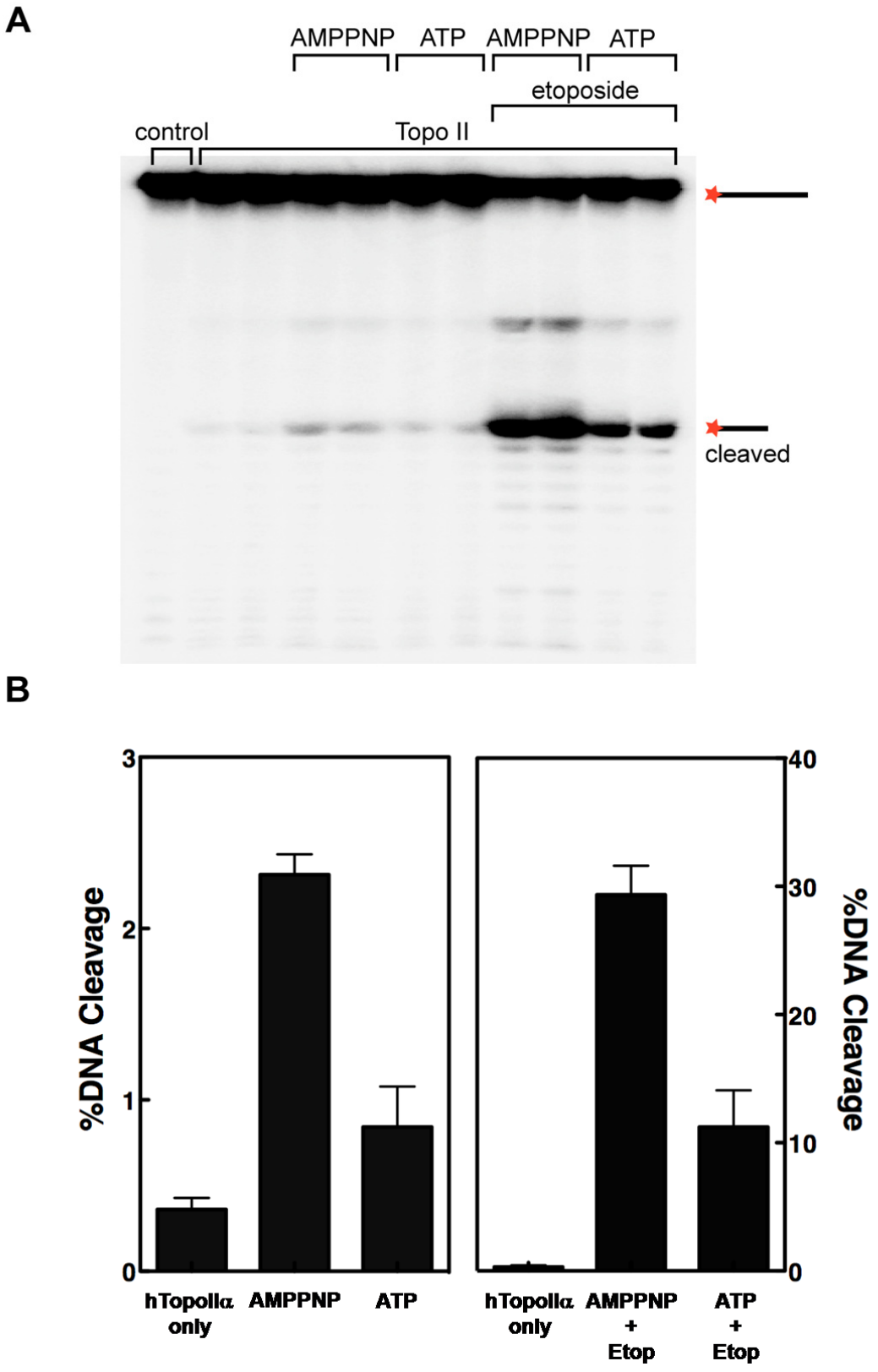

Effects of ATP and a non-hydrolyzable ATP analog (AMPPNP) on the cleavage of a radioactively labeled (top strand) clv oligonucleotide (without the fluorescent labels or

single-stranded tail) by hTopoIIα. (A) shows a representative polyacrylamide gel of duplicate experiments. Control represents the DNA oligonucleotide. Assays were carried out as indicated in the presence of 1 mM ATP, 1 mM AMPPNP, and/or 100 μM etoposide. The positions of the intact and cleaved oligonucleotide are indicated. (B) shows the quantification of two independent experiments done in duplicate or triplicate. Error bars represent standard deviations.

Fig. S19. The effect of ATP on DNA bending and opening

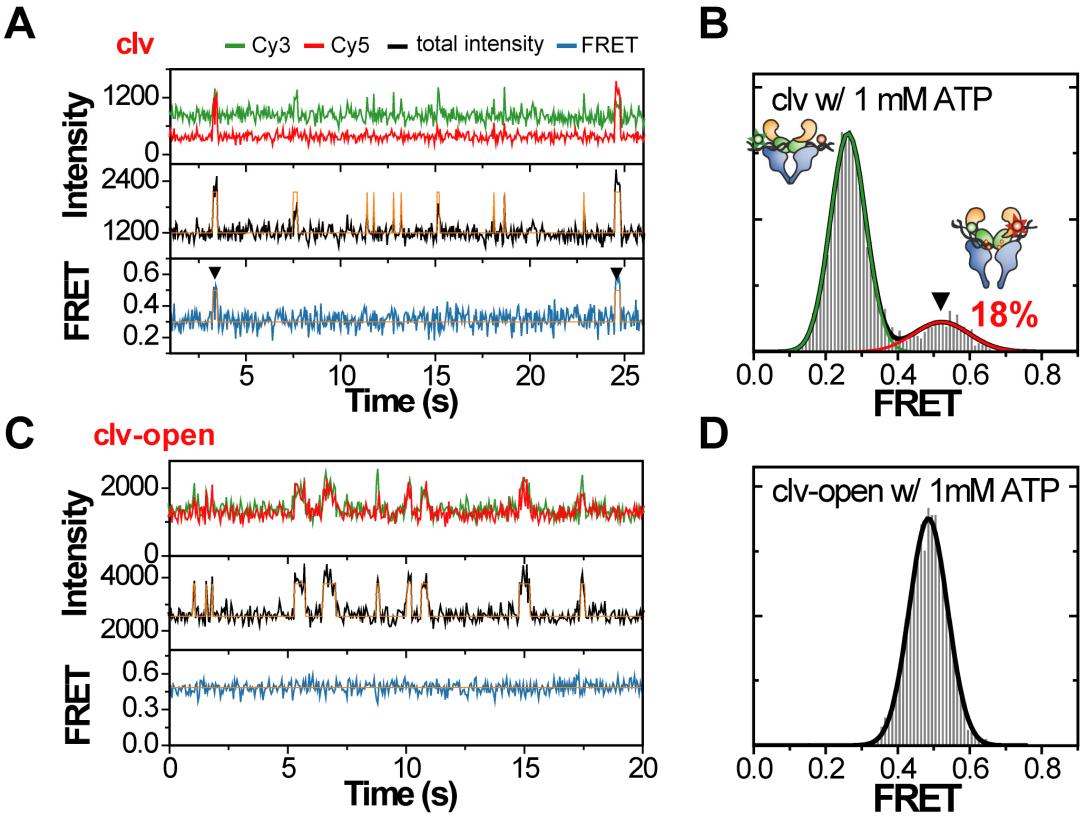

(A) Representative fluorescence intensity (top and middle) and FRET (bottom) time traces of clv in the presence of ATP (1 mM). (B) Corresponding FRET histogram of DNA duplex with bound enzyme. Compared to Fig. 5B, no dramatic change was observed. (C) Representative fluorescence intensity (top and middle) and FRET (bottom) time traces of clv-open in the presence of ATP (1 mM). (D) Corresponding FRET histogram of DNA duplex with bound enzyme. Compared to Fig. 5H, no appreciable change was observed. The experiments were performed with 5 nM hTopoIIα and 5 mM Mg^{2+}. Histograms were fitted to Gaussian functions.

Fig. S20. Operational model of type IIA topoisomerases

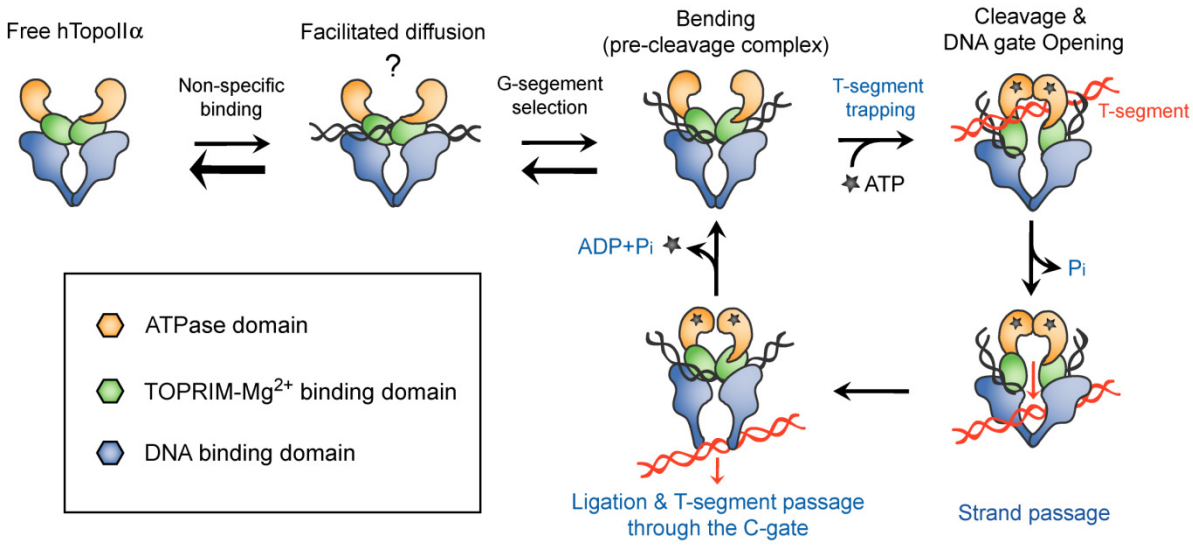

On the basis of our observation, we propose a model of sequential topoisomerase II operations: non-sequence specific DNA binding, facilitated diffusion, selection of G-segment through sequence-specific Mg^{2+}-dependent DNA bending, and cleavage and opening of G-segment DNA stimulated by N-gate clamping. There are still questions as to how the trapping event of the T-segment is communicated to regulate N-gate clamping, ATP-hydrolysis, and other steps of the topoisomerase II catalytic cycle (blue texts).